Hindawi Publishing Corporation
Journal of Nanomaterials
Volume 2014, Article ID 275197, 9 pages
http://dx.doi.org/10.1155/2014/275197

*Research Article*

# Platinum(0)-1,3-divinyl-1,1,3,3-tetramethyldisiloxane Complex as a Pt Source for $Pt/SnO_2$ Catalyst

**Agnieszka Martyla,[1] Maciej Kopczyk,[1] Piotr Marciniak,[2] and Robert Przekop[3]**

[1] *Institute of Non-Ferrous Metals Division in Poznan, Central Laboratory of Batteries and Cells, 12 Forteczna Street, 61-362 Poznan, Poland*
[2] *Poznan Science and Technology Park of Adam Mickiewicz University Foundation, 46 Rubiez Street, 61-612 Poznan, Poland*
[3] *Centre of Advanced Technologies Adam Mickiewicz University, 6 Grunwaldzka Street, 60-780 Poznan, Poland*

Correspondence should be addressed to Agnieszka Martyla; agnieszka.martyla@claio.poznan.pl

Received 10 January 2014; Revised 13 March 2014; Accepted 27 March 2014; Published 27 April 2014

Academic Editor: Sylwia Mozia



This paper presents new preparation method of $Pt/SnO_2$, an important catalytic system. Besides of its application as a heterogenic industrial catalyst, it is also used as a catalyst in electrochemical processes, especially in fuel cells. Platinum is commonly used as an anode catalyst in low temperature fuel cells, fuelled with alcohols of low molecular weight such as methanol. Platinum(0)-1,3-divinyl-1,1,3,3-tetramethyldisiloxane complex was used as a precursor of metallic phase. The aim of the research was to obtain a highly active in electrochemical system $Pt/SnO_2$ catalyst with low metal load. Considering small size of Pt crystallites, it should result in high activity of $Pt/SnO_2$ system. The presented method of $SnO_2$ synthesis allows for obtaining support consisting of nanoparticles. The effect of the thermal treatment on activity of $Pt/SnO_2$ gel was demonstrated. The system properties were investigated using TEM, FTIR (ATR), and XRD techniques to describe its thermal structural evolution. The results showed two electrocatalytical activity peaks for drying at a temperature of 430 K and above 650 K.

## 1. Introduction

The hydrosilylation reaction as practiced industrially employs silicone-soluble, low-valent platinum catalysts called Karstedt's catalyst which is a platinum divinyl tetramethyl disiloxane complex, typically containing about one-weight percent of platinum in an organic solvent, Figure 1.

It is known that solutions of Karstedt's catalyst (Pt(dvs)) thermally decompose with deposition of platinum [1]. This property may be used effectively in formation of metallic phase precursors [1] from such molecular complexes when applying CVD [2] or PVD technique [3]. Typically, an organometallic precursor of the desired metal is vaporized and deposited on a surface, hot enough to decompose the precursor, resulting in deposition of the metal and release of the precursor ligands. Many of the CVD precursors are potential candidates for a low temperature metal deposition process. These metal precursors are frequently highly soluble in organic media and decompose at moderate temperatures or even under mild UV irradiation conditions [1].

Formation of metallic phase in a low temperature process could compete with traditional methods, in which a high temperature treatment plays a key role [4]. All platinum complexes decompose under oxidizing conditions at below 473 K. The vinyl complex, the so-called Karstedt's catalyst, was used to produce small Pt clusters [1, 5].

This report describes our first attempts to deposit platinum on $SnO_2$ support via low temperature processes. $Pt/SnO_2$ has been well-known in catalysis for years and used widely in reactions of reforming, CO, and alcohols oxidation [6–9]. Oxidation of alcohols is a reaction used in fuel cells that are an alternative form of obtaining energy. Their usage is still limited by deactivation of platinum catalyst [10–12] caused by methanol oxidation intermediates.

Alcohol oxidation is a multistage process taking place on an electrode surface [13] ((1)–(6)). Carbon dioxide developing

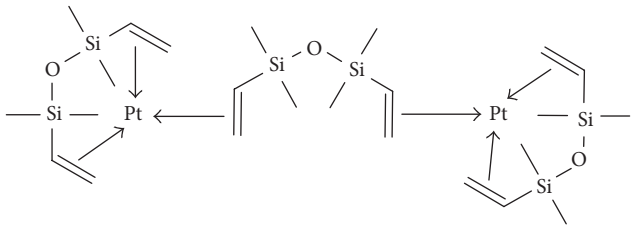


Figure 1: Karstedt's catalyst.

on the platinum and unoxidized intermediates block active sites and cause deactivation of the electrode.

*1.1. Dissociative Adsorption.* Consider

$$CH_3OH \longrightarrow CH_2OH + H^+ + e^- \quad (1)$$

$$CH_2OH \longrightarrow CHOH + H^+ + e^- \quad (2)$$

$$CHOH \longrightarrow COH + H^+ + e^- \quad (3)$$

$$COH \longrightarrow CO + H^+ + e^- \quad (4)$$

*1.2. Adsorbed Residues Reacts with an O-Containing Species.* Consider

$$CO + Pt(OH) \longrightarrow CO_2 + H^+ + e^- \quad (5)$$

$$H_2O + Pt \longrightarrow Pt(OH) + H^+ + e^- \quad (6)$$

Efforts to mitigate the poisoning effects of Pt have been concentrated on the addition of cocatalysts, particularly ruthenium and tin. Another way to improve the catalysts for the oxidation of CO and organic fuels is the production of Pt catalysts on oxide supports, which are highly stable in an oxidative medium of fuel cells [14–17].

The purpose of this work was to prepare catalyst $Pt/SnO_2$ systems with various contents of platinum from Karstedt's catalyst and to investigate the effect of the thermal treatment on the structural properties and electrocatalytic activity in the oxidation of methanol [9].

## 2. Preparation

*2.1. Preparation of $Pt/SnO_2$ by the Sol-Gel Technique.* The precursor of the tin(IV) oxide was tin(IV) acetate. To a mixture consisting of 48 $cm^3$ of isopropanol and 8 $cm^3$ of methanol 1.6 g of tin (IV) acetate was added and immersed in an ultrasonic bath at 323 K until tin (IV) acetate dissolved. Increasing amounts of xylene Pt(dvs) catalyst solution were added to the tin acetate alcohol solutions, corresponding to 13 mg and 26 mg of Pt to obtain samples containing 1.87 wt% (series A) and 3.74 wt% (series B) of Pt. After Pt(dvs) dosing, the systems were dispersed in an ultrasonic bath at 323 K for 24 hour. In these conditions, with no water added, a $SnO_2$ gel is formed by subsequent processes of transesterification (7), condensation (8), hydrolysis (9), and esterification (10) [18–20]:

$$Sn(CH_3COO)_4 + CH_3CH(OH)CH_3 \longrightarrow HOSn(CH_3COO)_3 + CH_3CH(H_3COO)CH_3 \quad (7)$$

$$2HOSn(CH_3COO)_3 \longrightarrow (CH_3COO)_3Sn{-}O{-}Sn(CH_3COO)_3 + H_2O \quad (8)$$

$$Sn(CH_3COO)_4 + H_2O \longrightarrow HOSn(CH_3COO)_3 + CH_3COOH \quad (9)$$

$$CH_3COOH + CH_3CH(OH)CH_3 \longrightarrow CH_3CH(H_3COO)CH_3 + H_2O \quad (10)$$

Next, the resulting gel was dried under vacuum for 48 h at a temperature of 293 K.

Series of samples containing 1.87% Pt (A series) and 3.74% Pt (B series) were heated under air atmosphere at temperatures: 373 K, 473 K, 573 K, 673 K, and 773 K using a temperature gradient 20 K/min, for 4 hours.

*2.2. Physicochemical Characteristics.* The phase identification and the influence of the thermal treatment on the $SnO_2$ phase were performed using a X-ray diffraction (XRD) powder diffractometer (Philips, PW 1050) using CuK$\alpha$ lamp radiation and a Ni filter. X-ray spectra were recorded in the angular range of 5 to 80 ($2\theta$). The Scherrer equation (11) was used to estimate the $SnO_2$ crystallite size. The equation shows that the crystallite size is inversely proportional to the peak width [21, 22]:

$$L = \frac{K\lambda}{\beta \cos\theta}, \quad (11)$$

where $L$ is an average crystallite size, $\lambda$ is the X-ray wavelength for Cu radiation ($\lambda = 1.5418$ Å), $\beta$ is the peak width of the diffraction peak profile at half maximum height resulting from a small crystallite, $\theta$ is the Bragg diffraction angle, and $K$ is a constant related to the crystallite shape.

The surface imaging was performed with Transmission Electron Microscopy (JOEL JEM 1200 EX).

The surface area of $Pt/SnO_2$ calcined at various temperatures was measured by $N_2$ adsorption using BET, with Micromeritics Instrument Corporation Model ASAP 2010. The sample, which was only dried, was outgassed at 293 K for 48 hours under vacuum. After calcinations, the samples were thoroughly outgassed at preparation temperatures for 24 hours.

The thermal analysis of $SnO_2$ gel was performed using a TA Instruments Gravimetric Analyzer (TA50) under a nitrogen and air atmosphere, 20 $cm^3$/min flow, at heat rate of 20 K/min in both cases.

Surface studies were carried out using a FT-IR spectrometer (Bruker, TENSOR 27) with ATR accessory (SPECAC). Measurements resolution was 4 $cm^{-1}$.

Table 1: Surface area of $Pt/SnO_2$ systems.

| Temperature | A series BET surface area ($m^2/g$) | B series BET surface area ($m^2/g$) |
|---|---|---|
| 773 K | 60 | 58 |
| 673 K | 78 | 74 |
| 573 K | 163 | 153 |
| 473 K | 231 | 219 |
| 373 K | 232 | 230 |
| 293 K | 23 | 27 |

The cyclic voltammetry (CV) experiment was performed in a two-electrode Swagelok type cell with the application of ECLAB V10.12 VMP model 0.3 potentiostat/galvanostat by Bio-Logic in the potential range of −0.5 to 1.0 V. The scan rate of 0.05 mV/s was applied.

The catalyst powders were suspended in a solution of PVdF-HFP in acetone with graphite and applied onto a stainless steel electrode Steel-$Pt/SnO_2$ |separator| Steel. The electrolyte contained 1 mol/$dm^3$ of $H_2SO_4$ and 2 mol/$dm^3$ of $CH_3OH$.

## 3. Results and Discussion

Structural and morphological properties of the materials were performed to study the effect of the temperature and the concentration of platinum on their catalytic activity. The studies of surface area show that the temperature has a significant effect on the change in surface area of received systems. Samples dried at room temperature have small surface area (Table 1) which proves the nonporous structure. The thermal treatment at 373 K results in a rapid increase in surface area which is characteristic for most systems obtained by a sol-gel method [23]. For high-temperature treatment, we observe a gradual decrease in surface area, up to about 60 $m^2/g$ (after treatment at 773 K). It should be noted that the specific surface area values are significantly higher than for the other porous tin(IV) oxides [24].

The first XRD pattern for all systems is typical for the as-synthesized air-dried gel product (Figure 2). This treatment results in a predominantly amorphous structure (Table 2). After heating (in air atmosphere, temperatures from 373 K to 773 K), according to the X-ray diffraction data, the $Pt/SnO_2$ samples consist of single phase, corresponding to the rutile-like structure with a tetragonal crystalline lattice. At higher temperatures, as a result of nanocrystalline $SnO_2$ formation, the diffraction peaks become progressively more intense and sharp. A typical tendency of crystallites growth with the temperature was observed (Table 2). The XRD patterns for B series are omitted since they represent analogical progression.

The change in the $SnO_2$ crystallites size calculated using Scherrer equation and estimated from micrographs shows similar correlation as a function of temperature.

Miller indexes are indicated on each diffraction peak. The reflection peaks at ~26 (2theta)/{110}, ~33 (2theta)/{101}, ~51 (2theta)/{211}, and ~65 (2theta)/{301} can be readily assigned

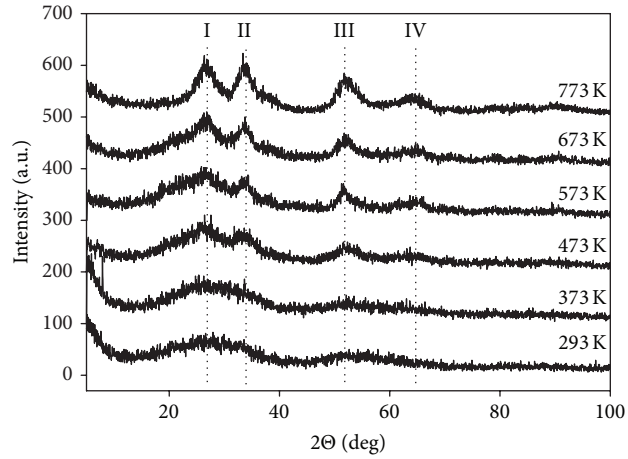


Figure 2: XRD patterns of 1.87% $Pt/SnO_2$ systems.

to a rutile-type tetragonal structure of $SnO_2$ (PDF 4+ Card File number 04-003-5853).

There are no noticeable reflexes of platinum. We believe that it is related to the small size of platinum crystallites which cannot be detected [25] using XRD method and at those concentrations.

Changes in crystallite morphology and support grains due to the change in temperature were observed with TEM (Figures 3 and 4). Images have dimensions 200 × 200 nm. The data of transmission electron microscopy exhibited a narrow size distribution of particles with an average diameter of 2 (Figure 4(b)) to 6 nm (Figure 3(f)). For sample, after treatment at 373 K (Figures 3(a) and 4(a)), the particle size is very small, which is approximately similar to the microscope image of Karstedt's complex after the evaporation of solvent form the solution [26]. With the increase in heating temperature, it can be seen that the $SnO_2$ nanoparticles' size slightly rises (Figures 3(e), 3(f), 4(e), and 4(f)).

On the basis of XRD measurements and microscopy, the presence of Pt crystallites larger than 1 nm was excluded. $SnO_2$ support crystallites of 2 to 10 nm size depending on processing temperature are only observed. In the synthesis method used for preparation, decomposition of metal precursor and formation of nanocrystalline $SnO_2$ occur simultaneously. The use of Pt divinyl complex instead of $H_2PtCl_6$ [27] significantly affects the size of metallic Pt clusters. The use of hexachloroplatinic acid and *incipient wetness impregnation* method results in Pt crystallites larger than 2.5 nm [28, 29] at the same loads.

Pt visualization on a support surface with XRD method is possible only in case of very high metal load, exceeding 10% [30–32]. When seeking explanation of that fact, we reminded about the stabilization possibility of small Pt clusters in presence of other oxide components in the metal/support system [33]. Also, the presence of small quantity of silica on a surface of tin dioxide increases activity of supported metal catalysts [34]. Hypothetical illustration of that phenomenon is presented in Figure 5.

Table 2: Crystallite size of $SnO_2$ calculated from XRD and TEM technique.

| Temperature | A series | | B series | |
|---|---|---|---|---|
| | XRD $SnO_2$ crystallite size (nm) | TEM $SnO_2$ crystallite size (nm) | XRD crystallite size (nm) | TEM $SnO_2$ crystallite size (nm) |
| 773 K | 4.4 | 9.3 | 4.5 | 10.4 |
| 673 K | 3.8 | 4.8 | 3.9 | 6.4 |
| 573 K | 2.5 | 3.1 | 2.8 | 4.4 |
| 473 K | 1.9 | 2.3 | 1.8 | 3.2 |
| 373 K | Noncrystalline solid | Noncrystalline solid | Noncrystalline solid | Noncrystalline solid |
| 293 K | Noncrystalline solid | Noncrystalline solid | Noncrystalline solid | Noncrystalline solid |

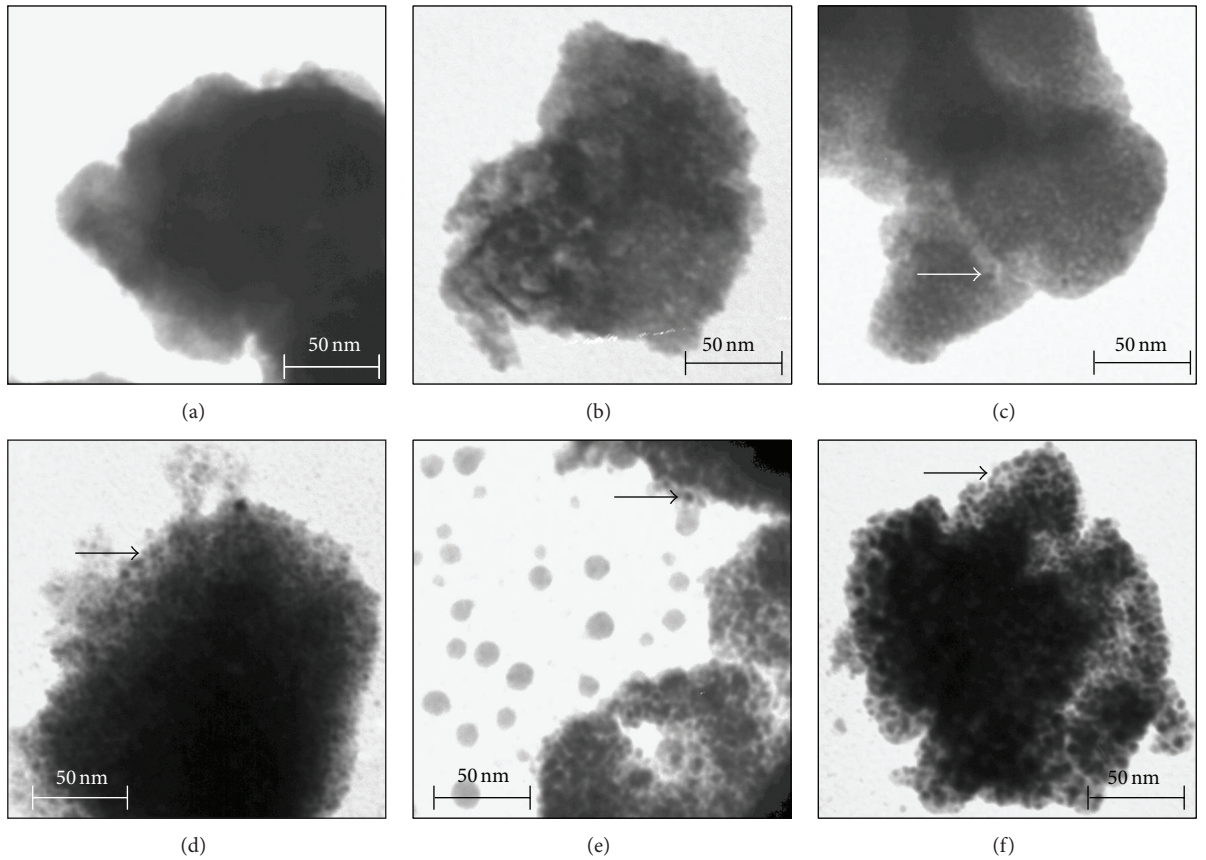


Figure 3: Pt/$SnO_2$ TEM images of A series: 1.87% Pt, after heating: (a) 293 K, (b) 373 K, (c) 473 K, (d) 573 K, (e) 673 K, and (f) 773 K. The visible area size is 200 × 200 nm. $SnO_2$ particles are matched.

Figures 6 and 7 show results of FTIR studies. The biggest changes in spectra occur in a 1000 to 1500 $cm^{-1}$ range after heating at 373–473 K. They result from removal of organic solvents residue from the bulk (isopropyl alcohol, acetic acid, and the corresponding ester). Fainting of bands d–h is correlated with decomposition of Pt complex at approximately 400 K. At the same time, appearance of a new band at 921 $cm^{-1}$, related to formation of $SiO_2$ (c) [35], can be observed. The peaks in the regions d—1018 $cm^{-1}$, e—1087 $cm^{-1}$ are the complex's band from the Si–O–Si stretching vibrations and they are observable only in case of higher initial Pt concentration systems.

A broad band between 500 and 772 $cm^{-1}$ (Figures 6 and 7(a, b)) is due to Sn–OH bond stretching.

The region of f (1255 $cm^{-1}$), g (1321 $cm^{-1}$), and h (1389 $cm^{-1}$) peaks is connected with C–O rocking, O–H bending vibrations, and C–H rocking. We observe a peak associated with the presence of acetic acid [36] (i) at about 1700 $cm^{-1}$. A broad band at 3400 $cm^{-1}$ (j) is attributed to the O–H stretching vibrations from residual alcohol, water, and SnO–H bonds.

For the annealed samples, the desorption of organics takes place, and the peaks at 3400 $cm^{-1}$ appear as a shoulder superimposed on the O–H band. The elimination of organic

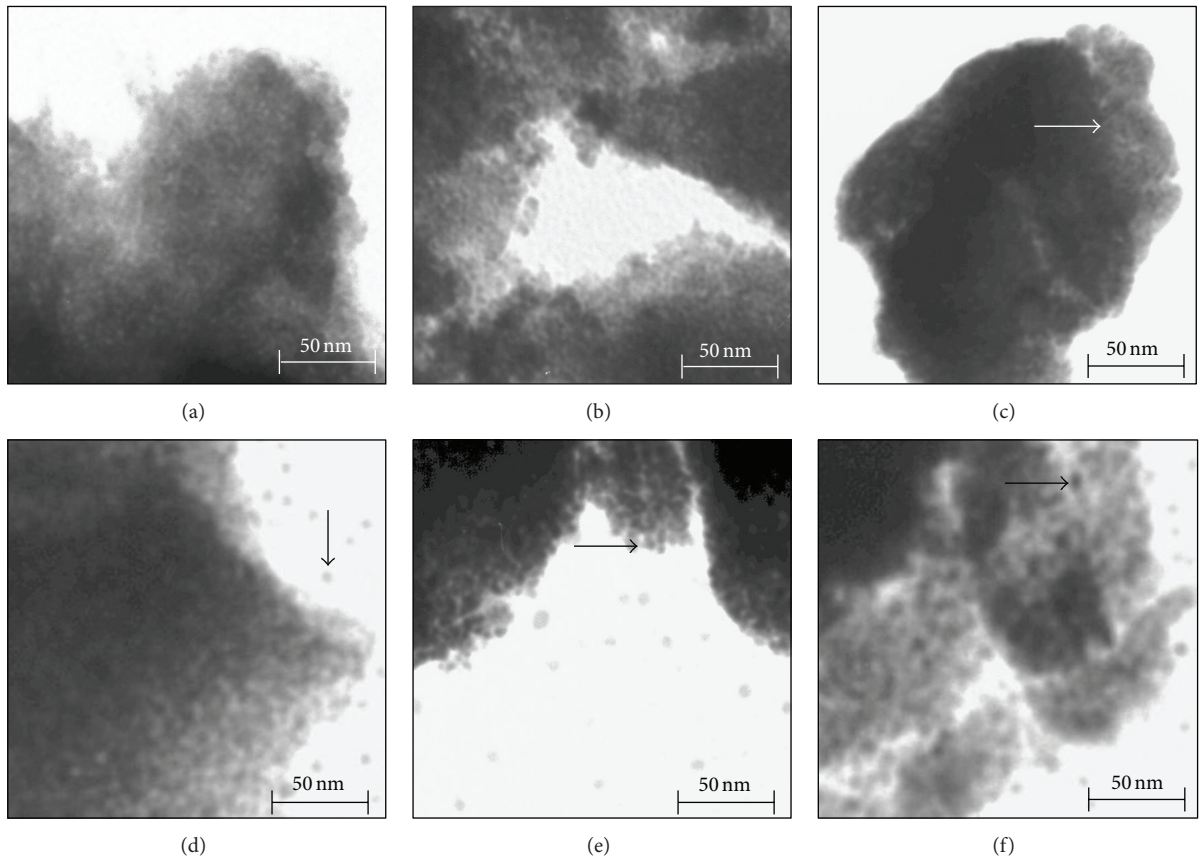


FIGURE 4: Pt/$SnO_2$ TEM images of B series: 3.74% Pt, after heating: (a) 293 K, (b) 373 K, (c) 473 K, (d) 573 K, (e) 673 K, and (f) 773 K. The visible area size is 200 × 200 nm. $SnO_2$ particles are matched.

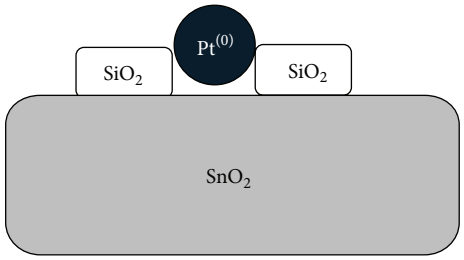


FIGURE 5: Hypothetical mechanism of small platinum particles stabilization by $SiO_2$.

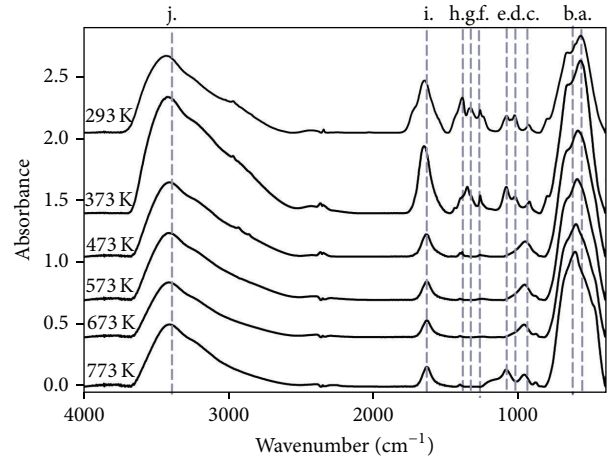


FIGURE 6: ATR/FT-IR spectra of 1.87% Pt on $SnO_2$ powders (A series).

residues provokes a change in intensity of the peak at 1650 $cm^{-1}$ (i). The absorption band from 500 to 772 $cm^{-1}$ decreases with the change in intensity of its components (a, b). The $SnO_2$ modes can be seen, with the Sn–O–Sn mode at 636 $cm^{-1}$, while a lattice mode of $SnO_2$appears at 772 $cm^{-1}$ [37].

Thermal decomposition of the starting gels in oxidizing atmosphere is presented in Figure 8. For both systems, the process occurred in several steps. Mass loss of about 5% at 330 K evidenced by the TG curve can be attributed to the removal of certain amount of organic solvents. Next steps are observed at 553 K and 610 K and they are linked with the further process of removing the organic solvents from the gel network [38]. The elimination of organic species was also observed in FTIR studies. For temperatures exceeding 620 K, no significant mass loss is visible. One can conclude that removal of solvents from the gel structure is accomplished. TG curve shows no distinct mass loss corresponding to Pt

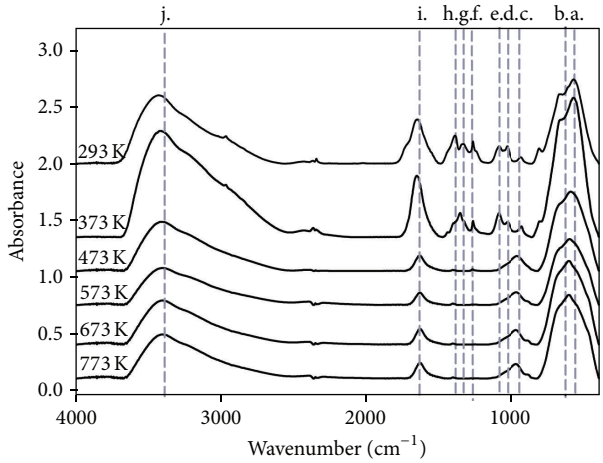


Figure 7: ATR/FT-IR spectra of 3.74% Pt on $SnO_2$ powders (B series).

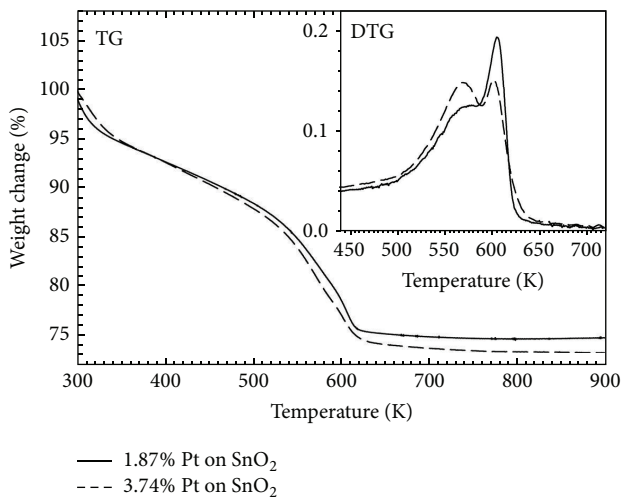


Figure 8: TG/DTG curves measured on $Pt/SnO_2$ powders vacuum dried at 293 K.

complex decomposition which should be localized in a 390–420 K range as one can expect from FTIR measurements and reference data [26]. This is due to a fact that mass loss linked to complex decomposition is a small fraction of the investigated system.

Cyclic voltammetry analysis is a good technique to obtain information about the functional properties of synthesized $Pt/SnO_2$ [17]. Electrocatalytic activity of $Pt/SnO_2$ in the methanol oxidation reaction is shown in Figure 9 which gives the cyclic voltammograms measured on 1.87% $Pt/SnO_2$ and 3.74% $Pt/SnO_2$.

Systems dried at room temperature show relatively low electrocatalytic activity (Figure 9, A1, B1). No peaks from methanol oxidation are observed. They appear in the next sample series only after heating at 373 K (Figure 9, A2, B2). For these systems, the lowest potential value was also noted. It can be seen that the potentials of methanol oxidation peaks for $Pt/SnO_2$ are shifted to the anodic region for both catalysts with the thermal treatment temperature. This may be associated with the crystalline form in which the main catalyst component, platinum, occurs.

According to references, the crystallites with orientation Pt {111} < Pt {100} < Pt {110} [39] exhibit the highest activity in methanol oxidation and they also exhibit characteristic responses [37].

Concluding from voltammetric curves, in this case the active crystallographic plane is {110}. The decrease in the $SnO_2$ grain size is accompanied by an increase in currents of both processes that occur in the fuel cell.

Above 400 K, Karstedt's complex decomposes forming silica and platinum. It allows to assume that small Pt clusters are stabilized by the formation of $SiO_2$. After thermal treatment at 393 K, the electrochemical activity of the system is related to Karstedt's complex in surrounding of $SnO_2$ gel. At 493 K, decomposition of the complex with formation of metallic Pt surrounded by the $SiO_2$ from the decomposed organometallic compound occurs.

To simplify that a $\Delta I$ parameter has been introduced. Its value is equal to the sum of an oxidation current and an absolute value of reduction current (12):

$$\Delta I = I_{ox} + \left|I_{red}\right|. \quad (12)$$

Plots (Figure 10) present values of $\Delta I$ of all obtained systems as a function of temperature. Independently from platinum content, both systems show comparable activity in methanol oxidation reaction. First, the maximal electrocatalytic activity for 430 K seems to be related to decomposition of Karstedt's complex, which occurs at about 400 K in oxidative atmosphere (Figure 8, see also Figure 10). As a result of complex decomposition, small clusters of Pt are formed and they are visible at TEM micrographs. It seems that the decrease in electrocatalytic activity observed above 460 K is related to changes in $SnO_2$ support, not to change in Pt dispersion. In many electrocatalytic processes, the role of structural factors such as nanoparticles orientation in catalytic activity was noticed [27]. The minimal electrocatalytic activity observed at circa 580 K corresponds to the maximal mass loss from DTG curves (Figure 8). This temperature range overlaps with the end of gel support formation (end of clear mass loss). The observed increase in activity can be caused by formation of a system in which the support phase starts to play an important role in electrocatalytic activity by increasing the electronic conductivity of the catalytic layer [27].

## 4. Conclusions

Siloxyl platinum complex (Pt(dvs)) allows obtaining tin(IV) oxide with high surface area and highly dispersed $Pt/SnO_2$ system. The presence of small amounts of $SiO_2$, formed after decomposition of the complex, may result in stabilization of platinum nanoparticles in $SnO_2$ gel structure. The metallic phase of systems does not tend to sinter and therefore maintain high electrochemical activity even after thermal treatment at 773 K.

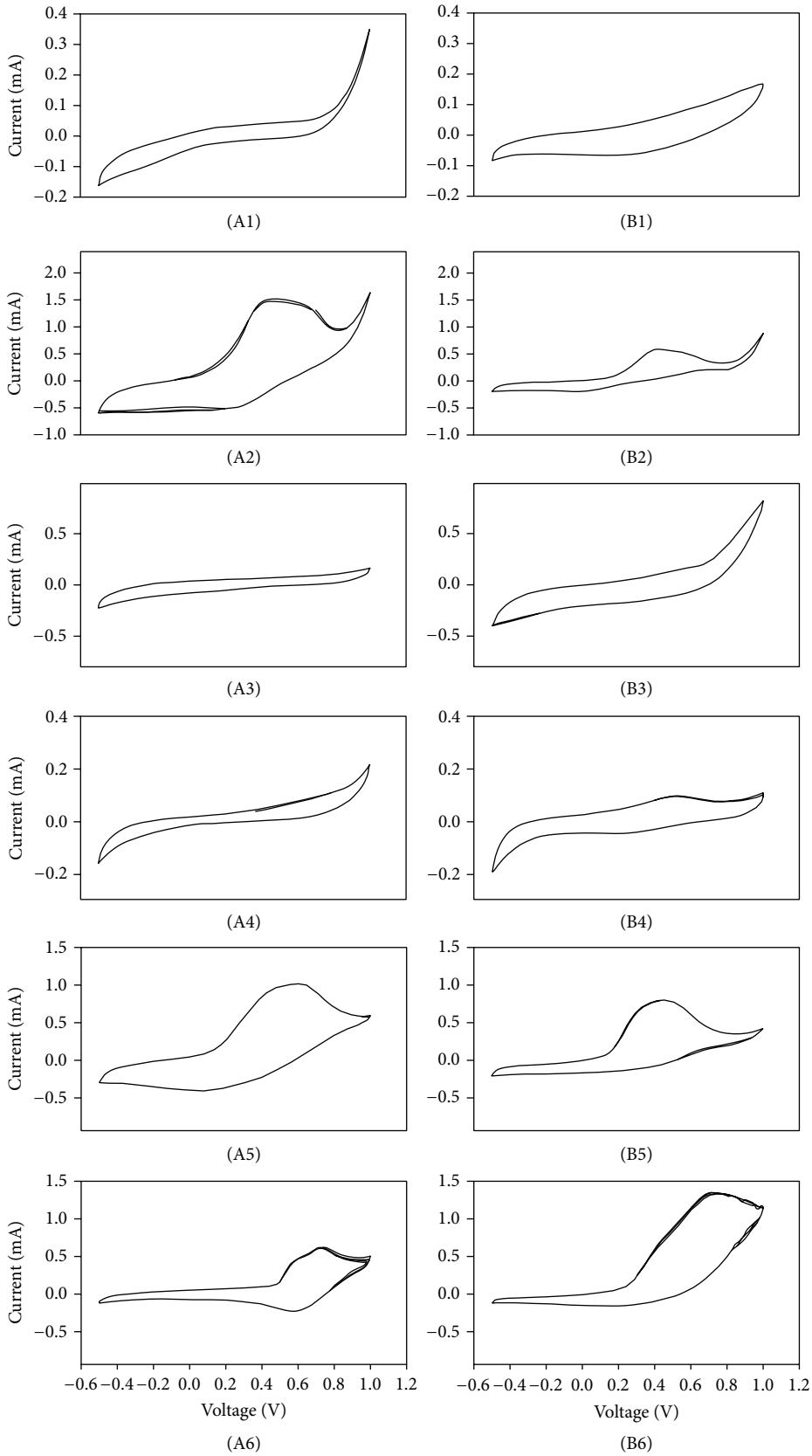


Figure 9: Cyclic voltammetry of the $Pt/SnO_2$ systems: (A) 1.87% Pt, (B) 3.74% Pt, after heating: 1: 293 K, 2: 373 K, 3: 473 K, 4: 573 K, 5: 673 K, and 6: 773 K.

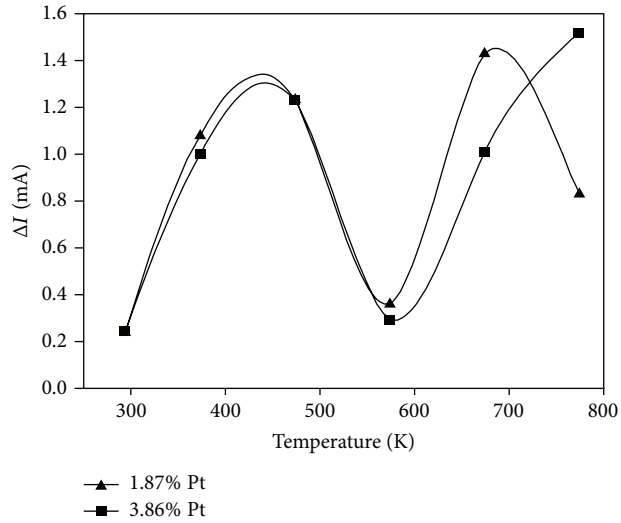


Figure 10: The sum of an oxidation current and an absolute value of reduction current as a function of temperature.

## Conflict of Interests

The authors declare that there is no conflict of interests regarding the publication of this paper.

## Acknowledgment

The study was financially supported by statutory activity of IMN Division in Poznan CLAiO no. 7001.01/BM/2013.

## References

[1] L. N. Lewis, K. H. Janora, J. Liu, S. Gasaway, and E. P. Jacobson, "Low temperature metal deposition processes for optoelectronic devices," in *Organic Photovoltaics V*, Z. H. Kafafi and P. A. Lane, Eds., vol. 5520 of *Proceedings of SPIE*, pp. 244–255, August 2004.

[2] J. R. Vargas Garcia and T. Goto, "Chemical vapor deposition of iridium, platinum, rhodium and palladium," *Materials Transactions*, vol. 44, no. 9, pp. 1717–1728, 2003.

[3] I. K. Igumenov, T. V. Basova, and V. R. Belosludov, "Volatile precursors for films deposition: vapor pressure, structure and thermodynamics," in *Application of Thermodynamics to Biological and Materials Science*, M. Tadashi, Ed., pp. 978–953, InTech, 2011.

[4] N. Kamiuchi, T. Mitsui, N. Yamaguchi et al., "Activation of $Pt/SnO_2$ catalyst for catalytic oxidation of volatile organic compounds," *Catalysis Today*, vol. 157, no. 1–4, pp. 415–419, 2010.

[5] K. Kinoshita, K. Routsis, and J. A. S. Bett, "The thermal decomposition of platinum(II) and (IV) complexes," *Thermochimica Acta*, vol. 10, no. 1, pp. 109–117, 1974.

[6] T. Kawaguchi, W. Sugimoto, Y. Murakami, and Y. Takasu, "Particle growth behavior of carbon-supported Pt, Ru, PtRu catalysts prepared by an impregnation reductive-pyrolysis method for direct methanol fuel cell anodes," *Journal of Catalysis*, vol. 229, no. 1, pp. 176–184, 2005.

[7] I.-S. Park, B. Choi, D.-S. Jung, and Y.-E. Sung, "Preparation and characterization of successively deposited Pt/Ru bimetallic electrocatalysts for the methanol oxidation," *Electrochimica Acta*, vol. 52, no. 4, pp. 1683–1687, 2006.

[8] N. Yamaguchi, N. Kamiuchi, H. Muroyama, T. Matsui, and K. Eguchi, "Effect of reduction treatment on CO oxidation over $Pt/SnO_2$ catalyst," *Catalysis Today*, vol. 164, no. 1, pp. 169–175, 2011.

[9] L. A. Frolova, Y. A. Dobrovolsky, and N. G. Bukun, "Oxide supported platinum electrocatalysts for hydrogen and alcohol fuel cells," *Russian Journal of Electrochemistry*, vol. 47, no. 6, pp. 697–708, 2011.

[10] R. Parsons and T. VanderNoot, "The oxidation of small organic molecules. A survey of recent fuel cell related research," *Journal of Electroanalytical Chemistry and Interfacial Electrochemistry*, vol. 257, no. 1-2, pp. 9–45, 1988.

[11] C. Lamy, A. Lima, V. LeRhun, F. Delime, C. Coutanceau, and J.-M. Léger, "Recent advances in the development of direct alcohol fuel cells (DAFC)," *Journal of Power Sources*, vol. 105, no. 2, pp. 283–296, 2002.

[12] L. A. Frolova and Y. A. Dobrovolsky, "Platinum electrocatalysts based on oxide supports for hydrogen and methanol fuel cells," *Russian Chemical Bulletin*, vol. 60, no. 6, pp. 1101–1111, 2011.

[13] V. S. Bagotzky, Y. B. Vassiliev, and O. A. Khazova, "Generalized scheme of chemisorption, electrooxidation and electroreduction of simple organic compounds on platinum group metals," *Journal of Electroanalytical Chemistry*, vol. 81, no. 2, pp. 229–238, 1977.

[14] G. R. Salazar-Banda, H. B. Suffredini, L. A. Avaca, and S. A. S. Machado, "Methanol and ethanol electro-oxidation on Pt-$SnO_2$ and Pt-$Ta_2O_5$ sol-gel-modified boron-doped diamond surfaces," *Materials Chemistry and Physics*, vol. 117, no. 2-3, pp. 434–442, 2009.

[15] H.-J. Chun, D. B. Kim, D.-H. Lim, W.-D. Lee, and H.-I. Lee, "A synthesis of CO-tolerant $Nb_2O_5$-promoted Pt/C catalyst for direct methanol fuel cell; its physical and electrochemical characterization," *International Journal of Hydrogen Energy*, vol. 35, no. 12, pp. 6399–6408, 2010.

[16] K.-S. Lee, I.-S. Park, Y.-H. Cho et al., "Electrocatalytic activity and stability of Pt supported on Sb-doped $SnO_2$ nanoparticles for direct alcohol fuel cells," *Journal of Catalysis*, vol. 258, no. 1, pp. 143–152, 2008.

[17] A. Sandoval-González, E. Borja-Arco, J. Escalante, O. Jiménez-Sandoval, and S. A. Gamboa, "Methanol oxidation reaction on $PtSnO_2$ obtained by microwave-assisted chemical reduction," *International Journal of Hydrogen Energy*, vol. 37, no. 2, pp. 1752–1759, 2012.

[18] P. Kirszensztejn, A. Kawałko, A. Tolińska, and R. Przekop, "Synthesis of $SiO_2$-$SnO_2$ gels in water free conditions," *Journal of Porous Materials*, vol. 18, no. 2, pp. 241–249, 2011.

[19] N. N. Khimich, B. I. Venzel', L. A. Koptelova, and I. A. Drozdova, "Acetic acid in sol-gel process of hydrolytic polycondensation of tetramethoxysilane," *Russian Journal of Applied Chemistry*, vol. 77, no. 2, pp. 290–294, 2004.

[20] N. N. Khimich, "Synthesis of silica gels and organic-inorganic hybrids on their base," *Glass Physics and Chemistry*, vol. 30, no. 5, pp. 430–442, 2004.

[21] P. Scherrer, "Bestimmung der Grösse und der inneren Struktur von Kolloidteilchen mittels Röntgenstrahlen," *Nachrichten von der Gesellschaft der Wissenschaften zu Gottingen*, vol. 26, pp. 98–100, 1918.

[22] J. I. Langford and A. J. C. Wilson, "Scherrer after sixty years: a survey and some new results in the determination of crystallite size," *Journal Applied Crystallography*, vol. 11, pp. 102–113, 1978.

[23] P. Kirszensztejn, A. Szymkowiak, A. Martyła, P. Marciniak, and R. Przekop, "Porosity of aluminium oxide-based binary systems obtained by sol-gel method," *Reaction Kinetics and Catalysis Letters*, vol. 82, no. 2, pp. 287–293, 2004.

[24] A. Gaber, M. A. Abdel-Rahim, A. Y. Abdel-Latief, and M. N. Abdel-Salam, "Influence of calcination temperature on the structure and porosity of nanocrystalline $SnO_2$ synthesized by a conventional precipitation method," *International Journal of Electrochemistry Science*, vol. 9, pp. 81–95, 2014.

[25] L. Mädler, T. Sahm, A. Gurlo et al., "Sensing low concentrations of CO using flame-spray-made Pt/$SnO_2$ nanoparticles," *Journal of Nanoparticle Research*, vol. 8, no. 6, pp. 783–796, 2006.

[26] L. N. Lewis, J. Stein, Y. Gao, R. E. Colborn, and G. Hutchins, "Platinum catalysts used in the silicones industry: their synthesis and activity in hydrosilylation," *Platinum Metals Review*, vol. 41, no. 2, pp. 66–75, 1997.

[27] H. Pang, C. Huang, J. Chen, B. Liu, Y. Kuang, and X. Zhang, "Preparation of polyaniline-tin dioxide composites and their application in methanol electro-oxidation," *Journal of Solid State Electrochemistry*, vol. 14, no. 2, pp. 169–174, 2010.

[28] D.-J. Guo and J.-M. You, "Highly catalytic activity of Pt electrocatalyst supported on sulphated $SnO_2$/multi-walled carbon nanotube composites for methanol electro-oxidation," *Journal of Power Sources*, vol. 198, pp. 127–131, 2012.

[29] H. Zhang, C. Hu, X. He, L. Hong, G. Du, and Y. Zhang, "Pt support of multidimensional active sites and radial channels formed by $SnO_2$ flower-like crystals for methanol and ethanol oxidation," *Journal of Power Sources*, vol. 196, no. 10, pp. 4499–4505, 2011.

[30] C. Xu and P. K. Shen, "Electrochamical oxidation of ethanol on Pt-$CeO_2$/C catalysts," *Journal of Power Sources*, vol. 142, no. 1-2, pp. 27–29, 2005.

[31] C. Xu, P. K. Shen, X. Ji, R. Zeng, and Y. Liu, "Enhanced activity for ethanol electrooxidation on Pt-MgO/C catalysts," *Electrochemistry Communications*, vol. 7, no. 12, pp. 1305–1308, 2005.

[32] H. Song, X. Qiu, F. Li, W. Zhu, and L. Chen, "Ethanol electrooxidation on catalysts with $TiO_2$ coated carbon nanotubes as support," *Electrochemistry Communications*, vol. 9, no. 6, pp. 1416–1421, 2007.

[33] W.-J. Kim, I. Y. Ahn, J.-H. Lee, and S. H. Moon, "Properties of Pd/$SiO_2$ catalyst doubly promoted with La oxide and Si for acetylene hydrogenation," *Catalysis Communications*, vol. 24, pp. 52–55, 2012.

[34] Y.-D. Wang, X.-H. Wu, Q. Su, Y.-F. Li, and Z.-L. Zhou, "Ammonia-sensing characteristics of Pt and $SiO_2$ doped $SnO_2$ materials," *Solid-State Electronics*, vol. 45, no. 2, pp. 347–350, 2001.

[35] W. L. Scopel, M. C. A. Fantini, M. I. Alayo, and I. Pereyra, "Local order structure of a-$SiO_xN_y$:H grown by PECVD," *Brazilian Journal of Physics*, vol. 32, no. 2A, pp. 366–368, 2002.

[36] A. Martyla, L. Majchrzycki, P. Marciniak, B. Sztorch, M. Kopczyk, and R. Przekop, "Otrzymywanie cienkich warstw $SnO_2$ dla fotowoltaicznych materiałów elektrodowych przy użyciu techniki zol-żel," *Chemik*, vol. 67, no. 12, pp. 1207–1216, 2013.

[37] M. Epifani, M. Alvisi, L. Mirenghi, G. Leo, P. Siciliano, and L. Vasanelli, "Sol-gel processing and characterization of pure and metal-doped $SnO_2$ thin films," *Journal of the American Ceramic Society*, vol. 84, no. 1, pp. 48–54, 2001.

[38] P. Kirszensztejn and A. Szymkowiak, "Thermal analysis of binary system $Al_2O_3$-$SnO_2$ obtained by sol-gel technique—part I: oxidative atmosphere," *Journal of Thermal Analysis and Calorimetry*, vol. 81, no. 1, pp. 35–39, 2005.

[39] T. Iwasita, "Fuel cells: spectroscopic studies in the electrocatalysis of alcohol oxidation," *Journal of the Brazilian Chemical Society*, vol. 13, no. 4, pp. 401–409, 2002.